

## Original Articles

## The seasonal and annual impacts of landscape patterns on the urban thermal comfort using Landsat

Li Feng<sup>a,\*</sup>, Menmen Zhao<sup>a</sup>, Yanan Zhou<sup>a</sup>, Liujun Zhu<sup>b</sup>, Huihui Tian<sup>a</sup><sup>a</sup> School of Geographic Science and Engineering, Hohai University, Nanjing 211100, China<sup>b</sup> Department of Civil Engineering, Monash University, 3800, Australia

## ARTICLE INFO

## Keywords:

Urban thermal comfort  
Modified temperature-humidity index (MTHI)  
Remote sensing data  
Spatio-temporal characteristics  
Landscape patterns

## ABSTRACT

The traditional in situ data based temperature-humidity indexes (THIs) have been widely used in the assessment of the quality of urban thermal environment, with the spatial details of thermal comfort currently unavailable. In this study, the THI is modified replacing the required in situ air temperature and relative humidity with remote sensing retrieved Land Surface Temperature and Normalized Difference Moisture Index, being the modified temperature-humidity index. The proposed remote sensing based index is then used to explore the spatio-temporal characteristics of urban thermal comfort, which are used to describe the urban thermal comfort grading in different seasons and the landscape metrics as well as to investigate the response of urban thermal comfort to landscape patterns seasonally and annually. The results show that at the macro scale, the impacts of landscape patterns on thermal comfort are the most important in summer with water bodies and built-up land being the most desirable and uncomfortable types, respectively. The opposite results are found in spring and winter despite the relatively less important effect in winter. At the micro scale, the variance contribution rate of the Percentage of Landscape to the MTHI is above 70%, and that of the Landscape Division Index and Aggregation Index is from 10% to 38.1%. It indicates that the composition of the landscape is the main factor affecting urban thermal comfort and is better than the landscape structure. The MTHI based on remote sensing data can monitor the spatial distribution of urban thermal comfort and is suitable to explain the reasons for the thermal comfort temporal variations.

## 1. Introduction

Urban thermal comfort is increasingly focused on because of the continuous deterioration of the urban environment resulted from rapid urbanization. The urban temperature-humidity and its seasonal change is the main characteristic of urban thermal comfort, which ties in with various aspects such as health risk (Parsons, 2013; Omonijo, 2017), living environment (Han et al., 2007; Xu et al., 2017; Alia and Patnaik, 2018), human behaviors (Thorsson et al., 2007; Cheng et al., 2010; Qiao et al., 2019) and urban design (Nikolopoulou and Steemers, 2003; Nikolopoulou and Lykoudis, 2006; Huynh and Eckert, 2012; Chen and Ng, 2012; Middel et al., 2014; He et al., 2015; Sun et al., 2017; Balogun and Daramola, 2019).

Urban thermal comfort is usually described by two categories of models. Empirical models have been developed and widely used in early studies using various indexes such as the effective temperature (ET) (Houghton and Yaglou, 1923), Wet Bulb Globe Temperature

(WBGT; Yaglou and Minard, 1957), and the discomfort index (DI; Thom and Bosen, 1959). Among those, the DI is the most popular one to assess the discomfort sensation and the health risk in populations, representing the joint effect of temperature and humidity (Tselepidaki et al., 1992; Zauli et al., 2008; Din et al., 2014; Xu et al., 2017). Meanwhile, the mechanism models were proposed by using the physical indexes such as the predicted mean vote (PMV; Fanger, 1970) and the physiological equivalent temperature (PET; Höppe, 1999). Horikoshi et al. (1995) proposed the effective temperature vote (ETV) index to describe the universal and separate effects of environmental variables simultaneously. Nagano and Horikoshi (2011) extended ETV for outdoor applications (known as ETVO) adding the shortwave component of solar radiation. The PET is usually employed to obtain the scenarios of thermal comfort, which is a product of fundamental environmental factors and their interactions (Matzarakis et al., 1999).

In addition to using these indexes to study urban thermal comfort, many researchers have investigated the impact of various single

\* Corresponding author at: Department of Geographic Information Science, School of Geographic Science and Engineering, Hohai University, Nanjing 211100, China.

E-mail address: [fly@hhu.edu.cn](mailto:fly@hhu.edu.cn) (L. Feng).

landscape type on urban thermal comfort such as urban green spaces (Picot, 2004; Abreu-Harbich et al., 2015; Algeciras et al., 2016; Sun et al., 2017; Wang et al., 2017; Toy and Kantor, 2017), buildings (Li et al., 2005; Kakon et al., 2010), shade (Lin et al., 2010; Makaremi et al., 2012; Nasir et al., 2013), and water surface (Steenneveld et al., 2014). Moreover, Yang et al. (2013) presented a comprehensive investigation of the independent impacts of different ground surfaces on a thermal environment. All these studies have revealed the effect of landscape composition. Despite the successful applications of traditional indexes, they are mainly based on the in-situ meteorological observations and cannot provide the spatial details of urban thermal comfort. How to investigate the spatio-temporal characteristics of urban thermal comfort and their relationships with landscape is still an open question.

The increasing capability of remote sensing in describing the spatial details and physical processes provides a great opportunity to understand the urban thermal environment on a fine spatial-temporal scale. The Land Surface Temperature (LST) and the Normalized Difference Moisture Index (NDMI) directly calculated from remote sensing data have a demonstrated potential of describing the air temperature and relative humidity respectively (Xu et al., 2017; Li et al., 2013). In addition, high spatial resolution land use and land cover can be achieved by remote sensing based classification algorithms conveniently (Zhang et al., 2018; Zou and Greenberg, 2019), being an effective venue to characterize the richness of different landscape types. However, those remote sensing measurements or indexes cannot be directly used in any of the aforementioned thermal comfort models. Remote sensing based air temperature and relative humidity retrieved methods are being developed (Xu et al., 2017; Li et al., 2013) but they still suffer from the uncertainty of the retrieval models and the need of site specific calibration. Accordingly, a proper way filling the gap between remote sensing direct measurements and traditional index is required. Therefore, two issues will be settled: 1) the new index for obtaining the spatio-temporal characteristics of urban thermal comfort; 2) the impacts of landscape patterns on urban thermal comfort on the dimension of time.

In this study, a novel framework is developed by utilizing remote sensing to evaluate urban thermal comfort. The traditional temperature-humidity index is modified by using LST and NDMI retrieved from remote sensing data, with the urban thermal comfort being graded at a fine scale in terms of the normalized modified temperature-humidity index. The city of Nanjing in China is employed as the study area. The relationships between various landscape metrics and urban thermal comfort at different seasons are investigated using the proposed index. Furthermore, the variance contribution rate of different landscape metrics to the proposed index is probed.

## 2. Study area, data source and image preprocessing

### 2.1. Study area

As the capital of Jiangsu province, the city of Nanjing ( $118^{\circ}46' E$ ,  $32^{\circ}03'N$ ) has a population of approximately 8.16 million and is located in the largest economic zone of China, the Yangtze River Delta. The city's administrative area is approximately  $6598 km^2$ , of which 46.50% is covered by vegetation. Nanjing has a humid subtropical climate that is heavily influenced by the East Asia Monsoon, resulting in a hot rainy summer and a cold wet winter.

In addition, with the increasing economic development and urbanization in Nanjing City, the population and the demand for urban construction land are growing very rapidly. There is a built-up area increase of  $524 km^2$  from 1990 to 2013. In this context, eight administrative districts in Nanjing are selected as the studied area and illustrated in Fig. 1, covering the major population.

### 2.2. Data sources

#### 2.2.1. Remote sensing data and image preprocessing

In this paper, the changes of thermal comfort in different seasons in Nanjing are analyzed. The seasonal division is mainly based on meteorological data. Nanjing has four distinct seasons, with relatively longer summer and winter. The highest temperature in Nanjing is observed in July and August, followed by June and September. The average temperature in September and June is lower than that in June and August, but still having some dates with high temperature ( $> 35^{\circ}C$ ). Therefore, the four months of June, July, August and September are summer. December, January and February have the lowest average temperature of  $-2.1^{\circ}C$ , being winter. March, April and May are spring; October and November are autumn. However, certain studies have indicated that the climate in Nanjing may be categorized into three seasons: summer, winter and transition seasons (Peng et al., 2016, 2018). Here, spring and autumn may be regarded as transition seasons because both the surface temperature and humidity are similar in spring and autumn, which is shown in Fig. 2. Therefore, only the spring is included in this study for simplicity.

According to the availability and quality (mainly depending on the cloud ratio) of remote sensing data, the images in three seasons (winter, spring and summer) in four time points of 1994, 2000, 2010 and 2013 are chosen. Twelve image scenes are used including ten Landsat 5/7 TM/ETM+ scenes and two successive Landsat 8 OLI/TIRS scenes. A brief summary of the Landsat images is shown in Table 1. In the preprocessing of geometric correction and fine registration, the image-to-image registration is performed using the image of March 23, 1993 as the benchmark. The root mean square error after correction is less than 1 pixel (30 m). For atmospheric correction, the physical model of Fast Line-of-sight Atmospheric Analysis of Spectral Hypercubes (FLAASH) is applied. The sub-images of the study area are obtained from the original Landsat images, covering the whole area of Nanjing.

#### 2.2.2. Land cover and land use data source

The distribution of five types of landscapes at four time points is obtained based on the aforementioned Landsat images (Fig. 3). Since the proportion of grassland is very minimal, the grassland and forest are merged into one class when the landscape metrics are calculated. The overall accuracy of four classified images is over 90%.

#### 2.2.3. Meteorological data

The meteorological data originate from Nanjing National Based Climate Station, including the daily average, the daily maximum and minimum of temperature, as well as the relative humidity. The station is located at  $118^{\circ}43' E$ ,  $32^{\circ}00'N$  from January 1960.1 to December 2007. Then it is moved to  $118^{\circ}54' E$ ,  $31^{\circ}56'N$  since January in 2008.

## 3. Methodology

### 3.1. Modifying the temperature-humidity index

The discomfort index (DI) (Thom and Bosen, 1959) was used to measure the degree of human discomfort that can effectively indicate the degree of heat sensitivity of the human body to temperature and humidity, which is defined as

$$DI = T_{\alpha} - 0.55(1 - 0.01RH)(T_{\alpha} - 58) \quad (1)$$

where  $T_{\alpha}$  is the air temperature in  $^{\circ}F$  and RH is the relative humidity in %. This index is usually used in the calculation of urban thermal comfort (Xu et al., 2017). In Hu et al., 2005, the DI was modified as

$$THI = 1.8T + 32 - 0.55 \times (1 - 0.01RH) \times (1.8T - 26) \quad (2)$$

where  $T$  is the air temperature in  $^{\circ}C$ . Currently, reliable THI and RH can be only provided by in-situ meteorological observations and thus cannot reflect the spatial characteristics of the thermal comfort. To this

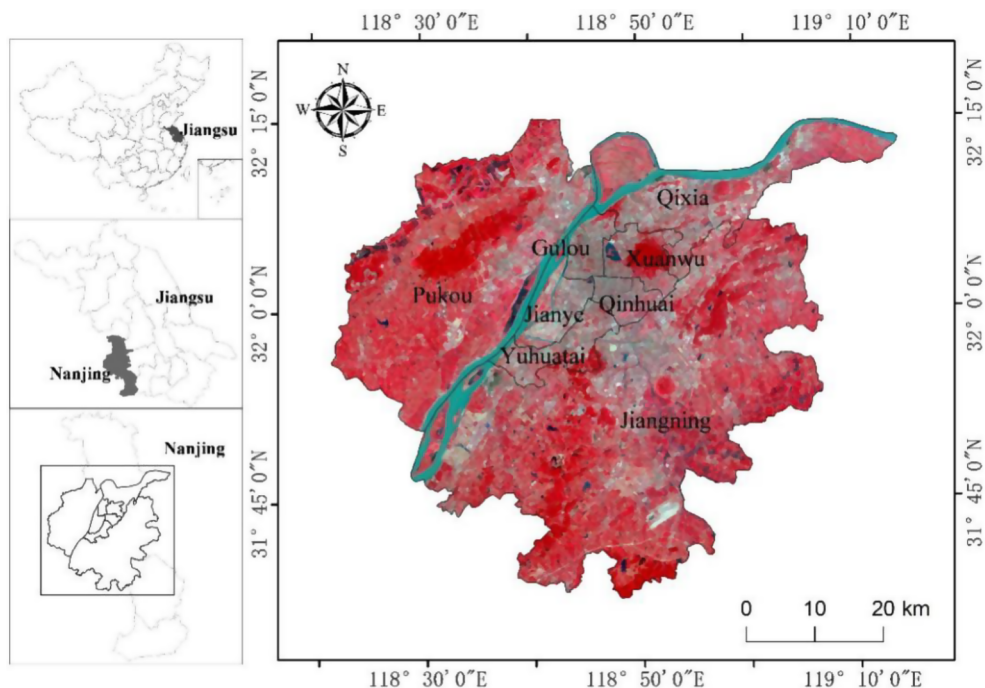


Fig. 1. Location of study area.

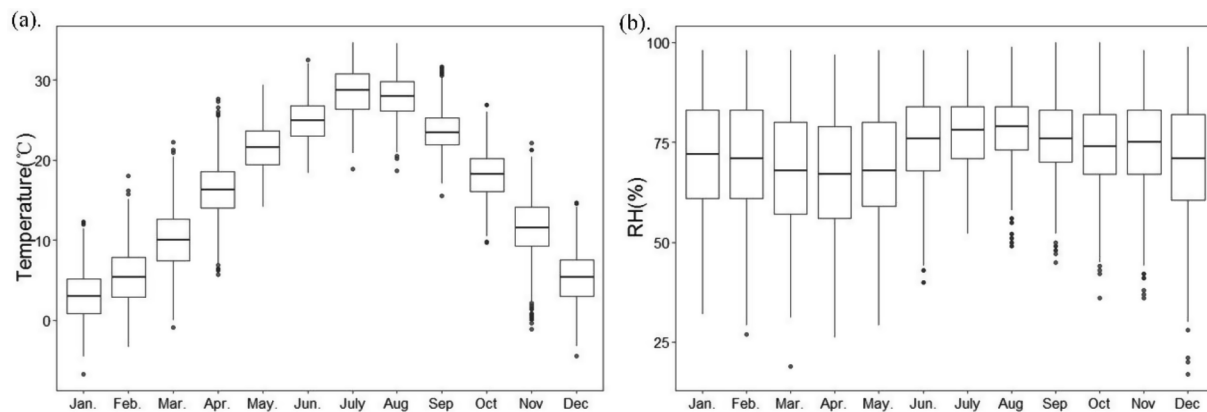


Fig. 2. The daily mean temperature (a) and relative humidity (b) in Nanjing during 1994–2014.

end, a new index, the modified temperature-humidity index (*MTHI*), is proposed by replacing the *THI* and *RH* with the Land Surface Temperature (*LST*) and the Normalized Difference Moisture Index (*NDMI*) respectively. The new remote sensing based index is thus:

$$MTHI = 1.8 \times LST + 32 - 0.55 \times (1 - NDMI) \times (1.8 \times LST - 26) \quad (3)$$

Only a brief introduction to the calculation of the *NDMI* and *LST* is provided, with detailed derivation being available in literature (Qin et al., 2001; Weng, 2009). *NDMI* can be obtained by the near infrared

(NIR) and short-wave infrared wavelengths (SWIR):

$$NDMI = \frac{NIR - SWIR}{NIR + SWIR} \quad (4)$$

*LST* may be presented as

$$LST = \{a(1 - C - D) + [b(1 - C - D) + C + D]T_b - DT_a\}/C - 273.15 \quad (5)$$

where  $T_a$  is the mean atmospheric temperature,  $a$  and  $b$  are constants and  $a = 67.355351$ ,  $b = 0.458606$ ,  $C = \varepsilon\tau$ , and  $D = (1 - \tau)$

**Table 1**  
Landsat data of different time points.

Data	Sensor	Data	Sensor		
Time point 1	1993-03-29 (spring)	Landsat TM	Time point 3	2010-04-05 (spring)	Landsat ETM +
	1994-07-22 (summer)	Landsat TM		2010-08-19 (summer)	Landsat TM
	1995-01-30 (winter)	Landsat TM		2010-12-17 (winter)	Landsat ETM +
Time point 2	2000-01-20 (winter)	Landsat ETM +	Time point 4	2012-04-26 (spring)	Landsat ETM +
	2000-04-17 (spring)	Landsat TM		2013-08-11 (summer)	Landsat OLI/TIRS
	2000-09-16 (summer)	Landsat ETM +		2014-01-02 (winter)	Landsat OLI/TIRS

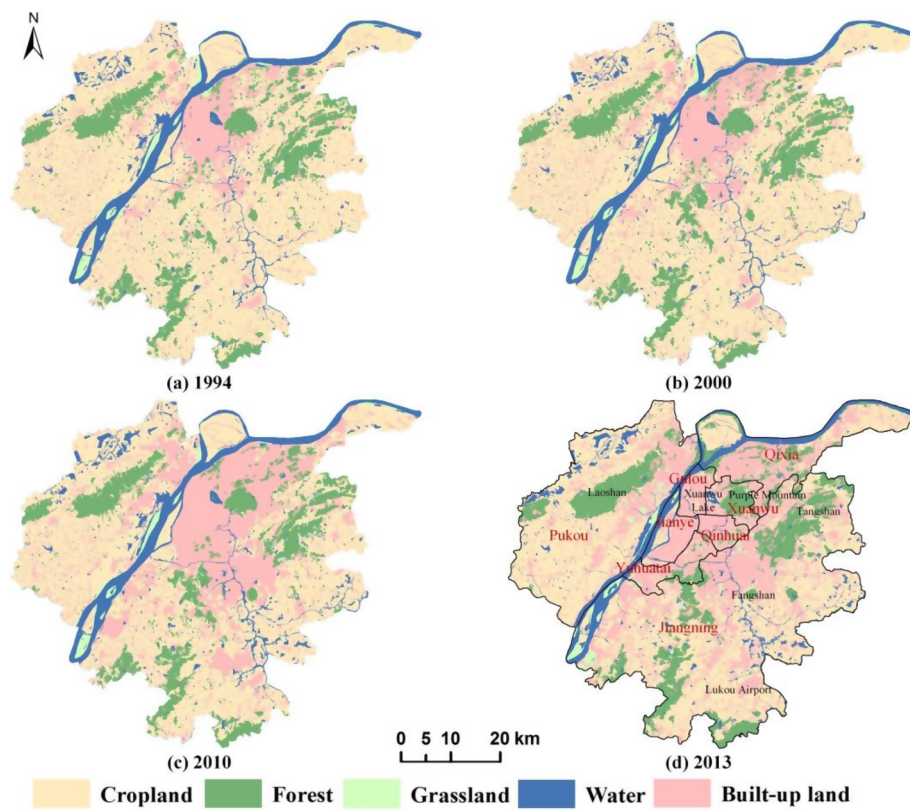


Fig.3. The distributions of five landscape types in four time points.

$[1 + (1 - \varepsilon) \tau]$ , here,  $\varepsilon$  and  $\tau$  are the land surface emissivity and atmospheric transmittance, respectively. In mid latitude,  $T_a = 16.0110 + 0.92621 \times T_o$  for summer while  $T_a = 19.2704 + 0.91118 \times T_o$  for winter.  $T_o$  is the near-surface air temperature.  $T_b$  is the brightness temperature corresponding to the radiation intensity observed by the sensor.

The LST can partly reflect the near surface air temperature with the same unit  $^{\circ}\text{C}$  of  $T_a$  (Li et al., 2013; Xu et al., 2017), which is generally larger than Ta at daytime. The replacement of air temperature with LST in the model is mainly based on the following facts: 1) LST is highly correlated with the air temperature and has been widely used in air temperature retrieval (Vancutsem et al., 2010; Xu et al., 2017); 2) in this context, the spatial patterns of the thermal comfort is rather the numerical values. Thus, the LST may be a convenient alternative to the more challenging air temperature observations; and 3) the transit time of the Landsat series in the study area is around 10:30 local time, and thus, the temperature measured at this time is close to the daily maximum temperature.

As shown in Eq. (4), NDMI (Hardisky et al., 1983) is calculated using the near infrared band and shortwave infrared band (Eq. (4)). Green vegetation has the largest reflectance at the near infrared band for the multiple scattering among leaves, while it has a much lower reflectance in the short infrared band because of the strong water absorption. The NDMI thus can be related to the vegetation water content and the water vapor nearby. Although this non-straightforward relationship is quite weak physically, many studies have confirmed its good correlation and consistency with relative humidity in meteorology (Li et al., 2013).

A comparison between the NDMI values and the relative humidity obtained by the weather station is shown in Table 2. The results show that an expected small difference of less than 0.1 is observed in most cases. A major difference can be observed because the relative humidity is the average value of that day. However, the NDMI describes the humidity condition at the satellite's transit time. Although there is a

**Table 2**  
Comparison the relative humidity of meteorological station and NDMI.

Date	NDMI	RH	$\Delta RH$
1993.3.29	0.75	0.55	0.20
1994.07.22	0.73	0.70	0.03
1995.01.30	0.73	0.63	0.10
1995.10.13	0.75	0.73	0.02
2000.01.20	0.69	0.65	0.04
2000.04.17	0.66	0.62	0.04
2000.09.16	0.63	0.55	0.08
2010.04.05	0.61	0.68	0.07
2010.08.19	0.64	0.68	0.04
2010.12.17	0.63	0.60	0.03
2012.04.26	0.65	0.45	0.20
2013.08.11	0.62	0.56	0.06
2014.01.02	0.57	0.47	0.10

quantitative relationship between the LST and the air temperature, there is no effective and reliable algorithm to directly convert the LST to the air temperature. Xu et al., 2017 proposed a technique to produce a fine-scale DI map by combining a Landsat thermal infrared image with in situ measured meteorological data. A regression analysis using the measured air temperature/relative humidity and an LST image was conducted. However, this method is not suitable in our study because there is only one state-run weather station in the study area.

### 3.2. Grading urban thermal comfort

#### 3.2.1. The method of grading

The physical meaning of the MTHI has changed compared with the THI although they have the high correlation as addressed above. So, the method of grading urban thermal comfort levels based on the THI (Hu et al., 2005) cannot be directly applied to applications using MTHI. Therefore, two steps are taken to implement the grading of the urban thermal comfort by using a relative grading method.

**Table 3**

Thermal comfort grading in different seasons.

Thermal comfort grading	Range of value in Winter and Spring	Range of value in Summer	Meaning (Relatively)
1	$1.5a < TI$	$TI \leq -1.5a$	More comfortable
2	$0.5a < TI \leq 1.5a$	$-1.5a < TI \leq -0.5a$	Comfortable
3	$-0.5a < TI \leq 0.5a$	$-0.5a < TI \leq 0.5a$	Less comfortable
4	$-1.5a < TI \leq -0.5a$	$0.5a < TI \leq 1.5a$	Discomfortable
5	$TI \leq -1.5a$	$1.5a < TI$	More uncomfortable

a is the standard deviation of  $TI$ .

1) Inspired by the concept of relative brightness temperature (Zhang et al., 2006), the MTHI is first normalized as:

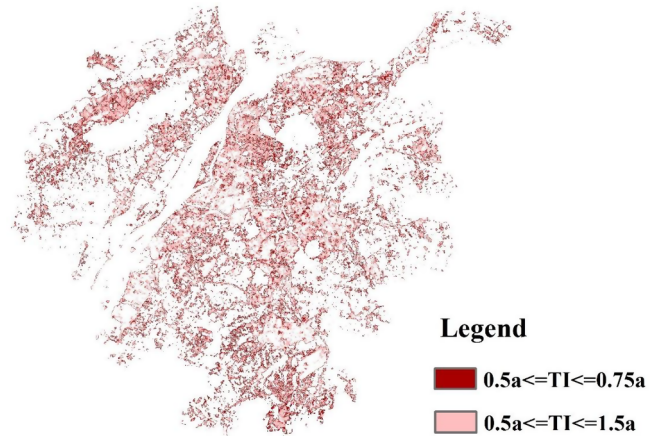
$$TI = \frac{MTHI - MTHI_{mean}}{MTHI_{mean}} \quad (6)$$

where  $TI$  is the normalized temperature-humidity index and  $MTHI_{mean}$  is the average value of the  $MTHI$ . This index indicates the thermal comfort of one location relative to the whole study area.

2) Similar to the methods of grading a heat island, i.e., the equidistant and the mean-standard deviation methods (Chen and Wang, 2009; Zhang et al., 2012), the thermal comfort based on the  $TI$  is graded into five levels. As shown in Table 3, the range of values in summer is opposite to that in winter and spring. The lower the value in summer, the more comfortable it is. The higher the value in winter and spring, the more comfortable it is.

### 3.2.2. Discussion on rationality of grading

At present, in the traditional method of grading urban thermal comfort, the threshold is determined in terms of the numerical results of the maximum, minimum, average and standard deviation of DI (Xu et al., 2017) or equal to interval division according to the results of the normalized temperature-humidity index (Li et al., 2013). Although these two methods can reflect the spatial distribution of thermal comfort, their thresholds, intervals and grades are determined subjectively which have some uncertainties. The mean-standard deviation method carries out the gradation based on the quantitative relationship between mean and standard deviation of different multiples which can better show the spatial distribution and temperature variation details of heat island. Therefore, referring to this method, comfort degree is divided into five grades by means of  $TI$ 's average value and standard deviation. The gradation here can protrude the spatial difference of thermal comfort degree. All the definitions of different comfort levels in Table 4 are relative, for example, more comfortable corresponds to relative more comfortable, and so on. In addition, taking the summer of 2013 as an example, the grading results with different the threshold

**Fig. 4.** Comparing the grading results with different threshold division.

division of uncomfortable (level 4) are compared, the results show that the changes of threshold division have a little impact (Fig. 4).

### 3.3. Calculating the different landscape metrics

Five landscape metrics, including the Percentage of Landscape (PLAND), Aggregation Index (AI), Landscape Division Index (DIVISION), Patch Cohesion Index (COHESION) and Shannon's Diversity Index (SHDI), are selected to reflect the landscape composition and the spatial structure (Table 4). The spatial pattern change of the landscape is widely acknowledged to be under the control of the ecological process at the macro scale, while the spatial pattern of the landscape varies according to the distribution of the patches on a micro scale (Wu, 2007). Accordingly, the investigation of the impacts of landscape composition and spatial structure on the thermal comfort is conducted on the macro and micro scales (Fig. 5).

**Table 4**

The detailed information of different landscape metrics.

Landscape metrics	Calculation formula and definition
Patch type level index	Percentage of Landscape
	$PLAND = p_i = \frac{\sum_{j=1}^n a_{ij}}{A} \times 100$ , $p_i$ is the proportion of landscape occupied by patch of type $i$ , $ij$ means the $j$ th patch of type $i$ , $a_{ij}$ is the area of patch $ij$ , $A$ is total landscape area; this index is the abundance ratio of a patch type in the landscape.
	Aggregation Index
	$AI = \left[ \frac{g_{ii}}{\max g_{ii}} \right] \times 100$ , calculation of AI for patch of type $i$ is based on the pixel edges $g_{ii}$ shared with itself, $\max g_{ii}$ is the largest number of possible edges shared for patch of type $i$ ; this index indicates the degree of aggregation between the patches.
Landscape Division Index	$DIVISION = \left[ 1 - \sum_{j=1}^n \left( \frac{a_{ij}}{A} \right)^2 \right]$ , $n$ is the number of patches of type $i$ , $ij$ means the $j$ th patch of type $i$ , $a_{ij}$ is the area of patch $ij$ , $A$ is total landscape area; this index indicates the degree of fragmentation of a patch.
	$COHESION = \left[ 1 - \frac{\sum_{j=1}^n p_{ij}}{\sum_{j=1}^n p_{ij} \sqrt{a_{ij}}} \right] \cdot \left[ 1 - \frac{1}{\sqrt{Z}} \right]^{-1} \times 100$ $n$ is the number of patches of type $i$ , $ij$ means the $j$ th patch of type $i$ , $p_{ij}$ is the perimeter of patch $ij$ , $a_{ij}$ is the area of patch $ij$ , $Z$ is the total number of grids in the landscape; this index indicates the natural connectivity of the related patch types.
Landscape level index	Shannon's Diversity Index
	$SHDI = -\sum_{i=1}^m (p_i \times \ln p_i)$ , $p_i$ is the proportion of landscape occupied by patch type $i$ , $m$ is the number of patch types in the landscape; this index can reflect the heterogeneity of landscape, the more balanced the proportion of the patch type area in the landscape, the more abundant the land use, the higher the $SHDI$ value.

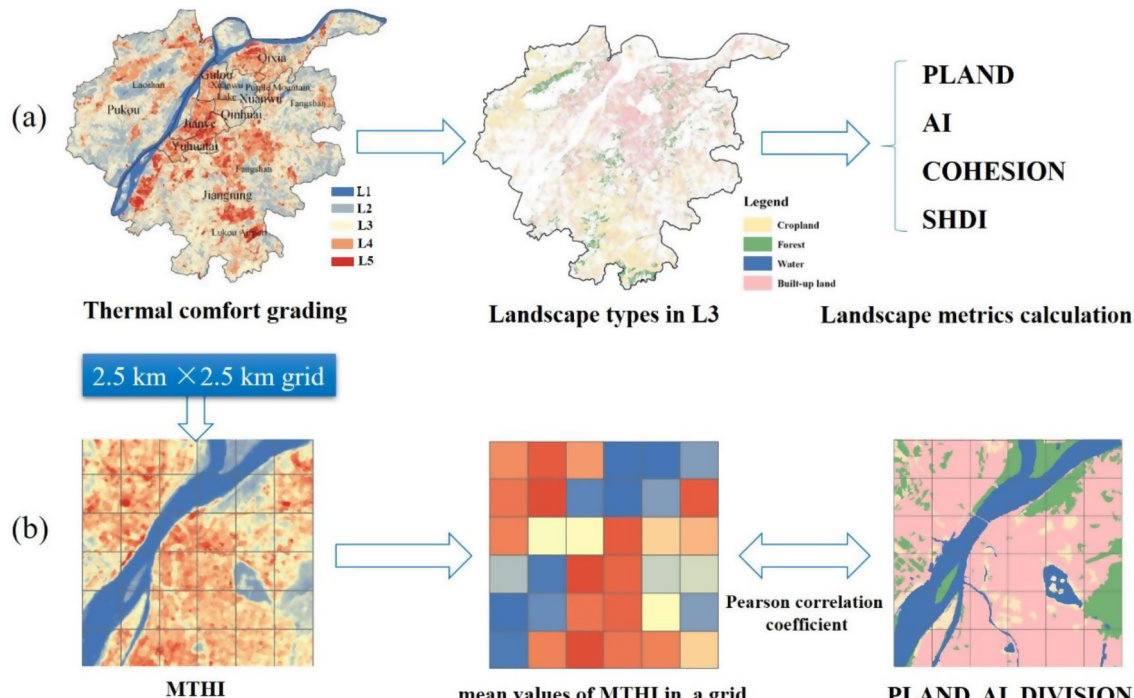


**Fig. 5.** Data processing on macro (a) and micro (b) scales, L1-5, respectively corresponding to more comfortable, comfortable, less comfortable, uncomfortable and more uncomfortable.

- At the macro scale, the classification of landscape types in different comfort levels can be obtained, e.g., different landscape types in level 3 (Fig. 5(a)), and then landscape metric of PLAND is used to analyze the impact of landscape composition on thermal comfort, while landscape metrics of AI, COHESION and SHDI are employed to investigate the impact of landscape structure on the thermal comfort levels.
- According to Yu et al. (2007), the 2.5 km scale can better reflect the overall landscape patterns of Nanjing City. Therefore, a 2.5 km × 2.5 km grid is selected as the research scale where the Pearson correlation between the mean values of MTHI and the landscape metrics, including PLAND, AI and DIVISION, is determined to show the correlation between thermal comfort and landscape composition, structure (Fig. 5(b)).

#### 3.4. Redundancy analysis (RDA)

The method of redundancy analysis (RDA) (Braak & Prentice, 1988) is a kind of linear analysis based on ranking technology, which can carry on statistical test of multiple explanatory variables effectively and independently maintain the variance contribution rate of each explanatory variable to the response variable. Compared with multiple linear regression, the method of redundancy analysis can more effectively separate the independent effects of various landscape factors.

To quantitatively evaluate the extent of impacts of different landscape metrics on urban thermal comfort on 2.5 km × 2.5 km grid, RDA is explored to calculate the variance contribution rate of different landscape metrics to the MTHI in summer seasons of four time points.

## 4. Results and analysis

### 4.1. The impacts of landscape composition on the thermal comfort levels

Fig. 6 shows the proportion of different landscape types (PLAND) at different levels of thermal comfort in each time point. Levels 1–5 denote more comfortable, comfortable, less comfortable, uncomfortable and more uncomfortable, respectively.

In summer, contrasting PLAND of different landscape types with five comfort levels in the same time point, the dominant landscape sorting in various levels is respectively (Fig. 6): level 1 (more comfortable): water body > forest > cropland > built-up land; level 2 (comfortable): cropland > forest > water body > built-up land; level 3 (less comfortable): cropland > built-up land > forest > water body; level 4 (uncomfortable) and level 5 (more uncomfortable): built-up land > cropland > forest > water body. The results indicate that the more the proportion of water body, cropland and forest is, the lower the comfort lever is; the more the proportion of built-up land is, the higher the comfort level is. The cropland and forest have the function of adjusting the thermal comfort and are inferior to that of water bodies. Through comparing PLAND of the same landscape type under five thermal comfort levels of four time points, PLAND of water bodies is the highest in level 1 (more comfortable) and then decreases from level 2 (comfortable) to level 5 (more uncomfortable), which indicates that a water body has obvious improvement on the thermal comfort (Fig. 6(c)). PLAND of the built-up land markedly increases as the thermal comfort worsen in summer (Fig. 6(d)). As the absolute dominant landscape type, the built-up land is the main reason for the deterioration of the urban thermal environment, which shows that urban construction has a great influence on urban thermal comfort. PLAND of water bodies and built-up land cause the opposite and important effects on the thermal comfort.

In winter and spring, water bodies have generally negative effects on the thermal comfort comparing in summer because PLAND of water bodies increases as the thermal comfort levels change from level 1 (more comfortable) to level 5 (more uncomfortable) (Fig. 6(c)). In contrast to water bodies, the impacts of built-up land on the thermal comfort are positive in these two seasons. In winter and spring, for cropland and forest, there are no overt disciplines such as water bodies and built-up land.

### 4.2. The impacts of landscape structure on the thermal comfort levels

The indexes of AI, COHESION and SHDI are calculated and used to analyze the impacts of landscape structure on urban thermal comfort (Figs. 7–9).

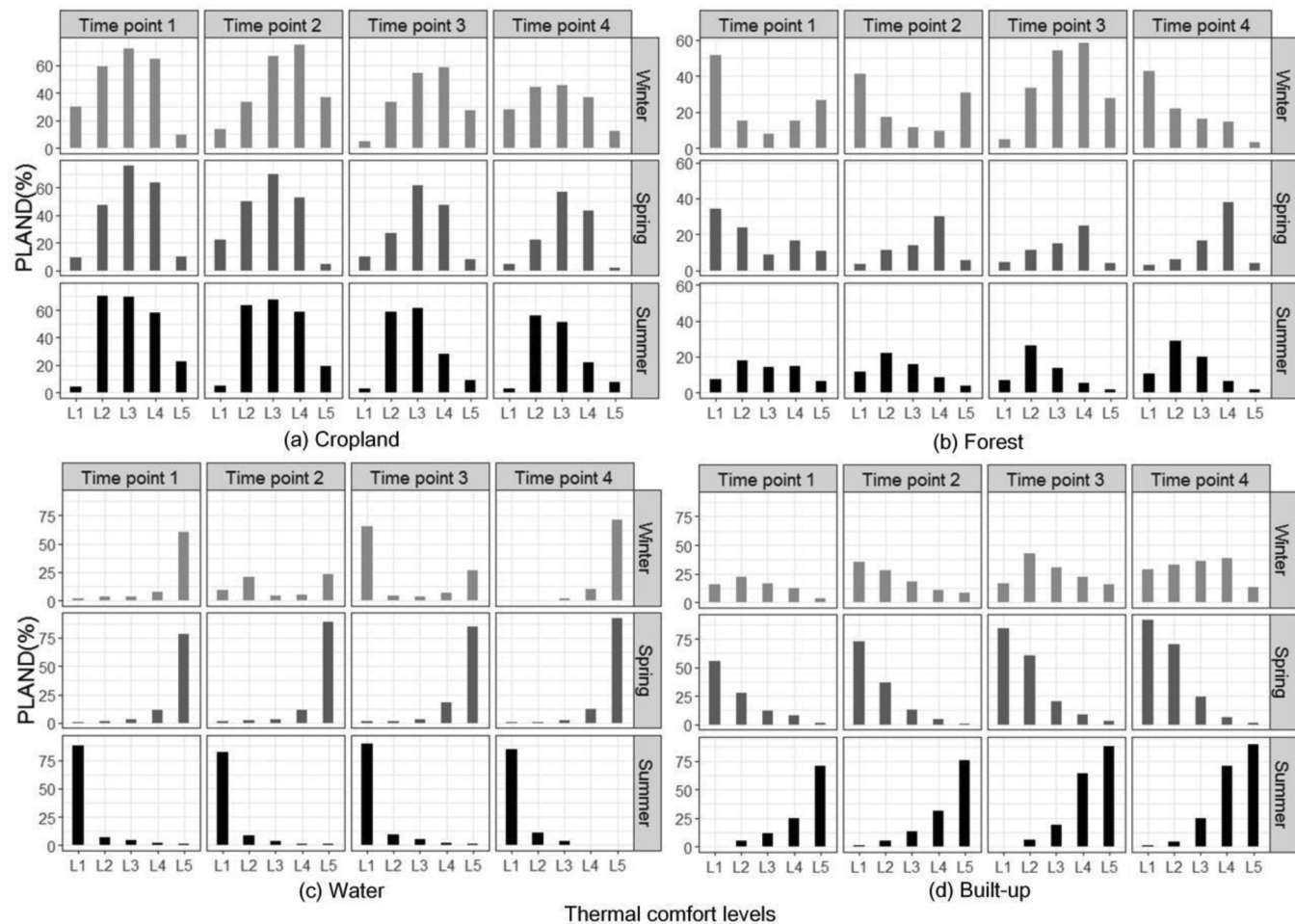


**Fig. 6.** PLAND of different landscape types, i.e., (a) cropland; (b) forest; (c) water; and (d) built-up land under different thermal comfort levels, L1–5, respectively corresponding to more comfortable, comfortable, less comfortable, uncomfortable and more uncomfortable.

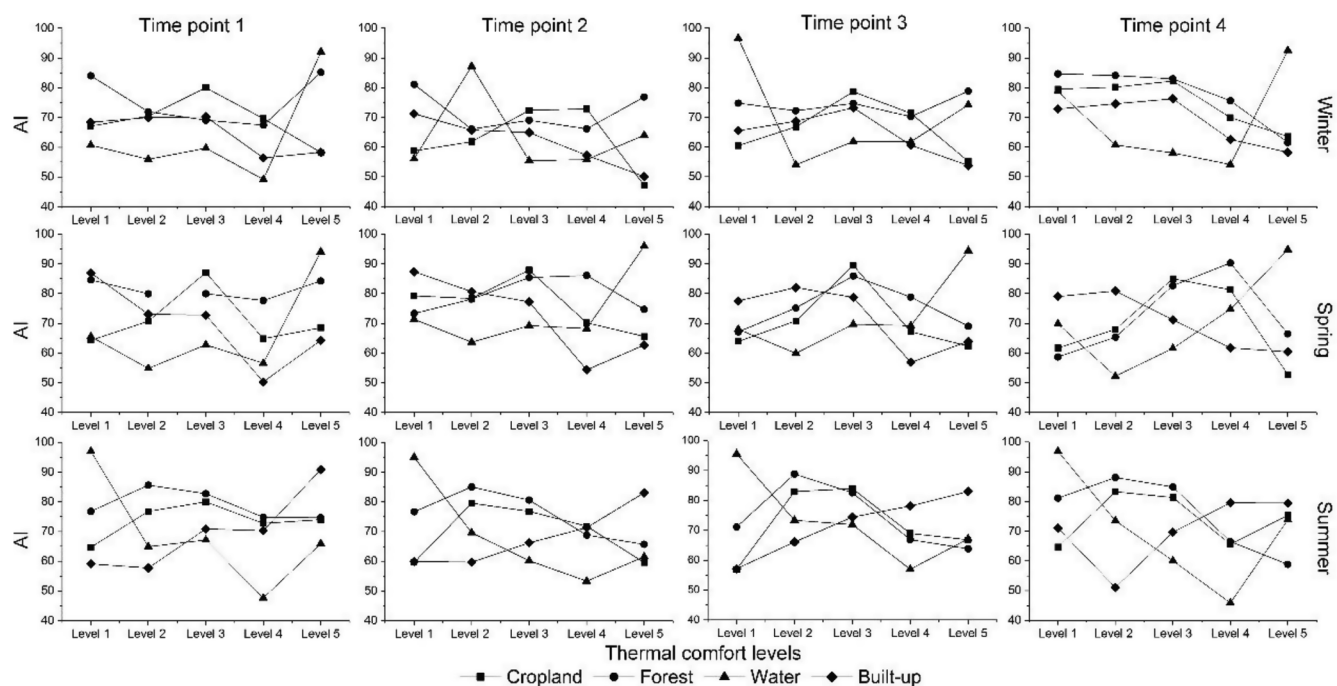


**Fig. 7.** Dynamic changes of AI of different landscape types under different thermal comfort levels, level 1–5, respectively corresponding to more comfortable, comfortable, less comfortable, uncomfortable and more uncomfortable.

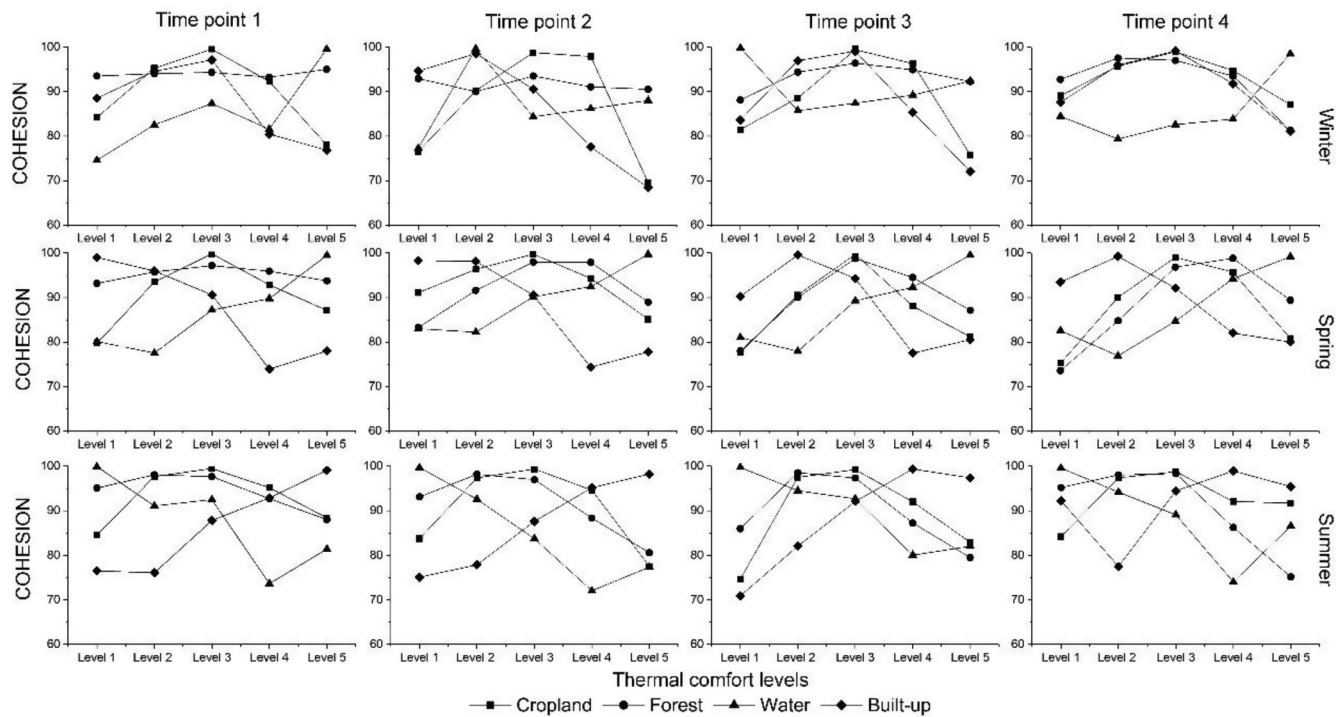


**Fig. 8.** Dynamic changes of COHESION of different landscape types under different thermal comfort levels, level 1–5, respectively corresponding to more comfortable, comfortable, less comfortable, uncomfortable and more uncomfortable.

In summer, AI and COHESION values of water bodies are the highest in level 1 (more comfortable). In contrast, the values of built-up land are the highest in level 5 (more uncomfortable), which indicates that the more concentrated distribution of water bodies has better effects on the improvement of thermal comfort; however, the more concentrated distribution of built-up land will make thermal comfort worse. AI and COHESION values of water bodies in level 5 (more uncomfortable) are higher than those in level 4 (uncomfortable), which can provide suitable insights that the effect of water bodies on the improvement of comfort degree will be restrained if there is a greater proportion and more concentrated distribution of built-up land around it. In addition, COHESION value of built-up land in level 5 (more uncomfortable) is lower than that in level 4 (uncomfortable) at time points 3 and 4. This finding is consistent with the worse thermal comfort caused by the large energy consumption and the high intensity of the heat source in the industrial park as well as the higher albedo and the high surface temperature in the new built-up area. In summer, the variation trend of AI and COHESION values of forest and cropland is similar. With the combination of PLAND, in the comfort zone, forest and cropland are the dominant landscapes, which indicates that a large

area of cropland and forest can also improve thermal comfort and that the forest has a better effect because AI and COHESION values of forest are larger than those of cropland in level 1 (more comfortable).

In winter, for water bodies, the great fluctuations of AI and COHESION values are prominent, which states that impacts of different types of water bodies (such as the Yangtze River, lake, or reservoir) on thermal comfort affected easily by the special weather. These values in spring are the highest in level 5 (more uncomfortable), which indicates that large stretches of water will make the surrounding colder and less comfortable. For built-up land, AI and COHESION values rapidly decline from level 4 which indicates that more scattered distribution of built-up land can make the place uncomfortable.

As the only landscape level index, Shannon's Diversity Index is selected in this study. According to Fig. 9, the relationship between SHDI and thermal comfort in winter is not significant. In spring and summer, the SHDI presents the trend of “low on both sides and high in the middle”. In level 1 (more comfortable) and level 5 (more uncomfortable), landscape type is comparatively single. In spring, the dominant landscape type in level 1 (more comfortable) is built-up land, and more than 70%~90% of landscape type is water bodies in level 5

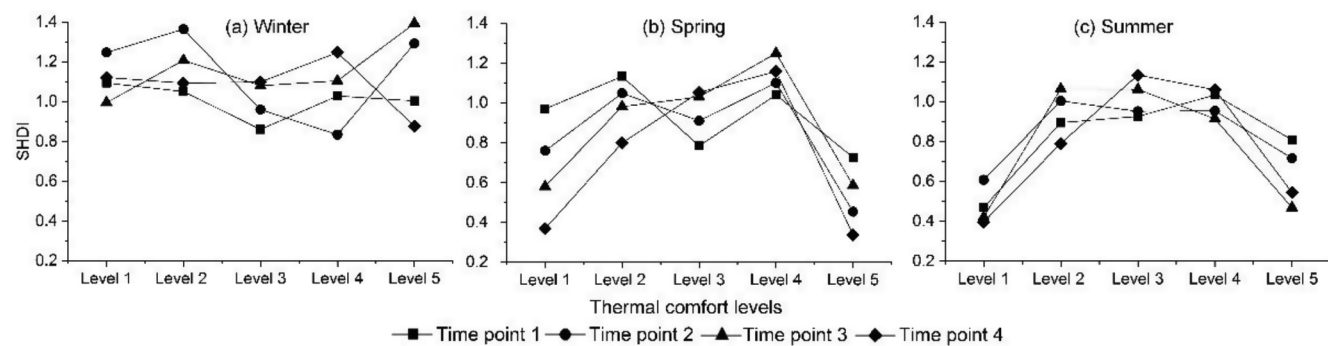


**Fig. 9.** Dynamic changes of SHDI of different seasons under different thermal comfort levels, level 1–5, respectively corresponding to more comfortable, comfortable, less comfortable, uncomfortable and more uncomfortable.

**Table 5**Correlation between MTHI<sub>mean</sub> and PLAND.

Landscape types	Time point 1			Time point 2			Time point 3			Time point 4		
	Winter	Spring	Summer									
Cropland	0.271**	-0.045	-0.130**	-0.690**	0.041	-0.020	-0.468**	-0.091	-0.354**	0.126**	-0.121**	-0.095*
Forest	-0.010	0.159**	-0.095*	0.243**	-0.178*	-0.231**	-0.044	-0.026	-0.212**	0.225*	-0.246**	-0.217**
Water	-0.648**	-0.647**	-0.516**	-0.297**	-0.662**	-0.602**	0.592**	-0.810**	-0.456**	-0.742**	-0.686**	-0.669**
Built-up	0.115*	0.586**	0.724**	0.431**	0.628**	0.723**	0.162**	0.615**	0.844**	0.079	0.751**	0.687**

\*\*A significant correlation at the level of 0.01 (bilateral).

\*A significant correlation at the level of 0.05 (bilateral).

**Table 6**Correlation between MTHI<sub>mean</sub> and AI.

Landscape types	Time point 1			Time point 2			Time point 3			Time point 4		
	Winter	Spring	Summer									
Cropland	0.064	-0.223**	-0.189**	-0.319*	-0.136**	-0.161**	-0.098*	-0.077	-0.117*	0.036	-0.238**	-0.169**
Forest	0.004	-0.044	-0.084	0.064	-0.112	-0.207**	-0.051	-0.045	-0.129**	0.118*	-0.394**	-0.336*
Water	-0.361**	-0.304**	0.235**	0.266**	-0.344**	-0.305**	0.399**	-0.393**	-0.189**	-0.265	-0.423**	-0.294**
Built-up	-0.082	0.368**	0.413**	0.569**	0.324**	0.354**	0.360**	0.386**	0.660**	0.005	0.362**	0.412**

\*\*A significant correlation at the level of 0.01 (bilateral).

\*A significant correlation at the level of 0.05 (bilateral).

(more uncomfortable). In contrast, in summer, in level 1 (more comfortable), more than 80% of landscape type is water bodies, and in level 5, more than 70% is built-up lands. In level 2, 3 and 4, land use types are abundant and fragmentation is high.

#### 4.3. Contribution of landscape composition and structure to thermal comfort at the micro-scale

##### 4.3.1. Correlation MTHI and landscape composition on the 2.5 km × 2.5 km grid

For calculating the correlation between thermal comfort and PLAND of different landscape types, the number of observations for all landscape types is 462. Table 5 presents the results at the micro-scale, and important conclusions can be obtained.

In summer, there is a negative correlation between MTHI and PLAND of cropland, forest and water bodies, which indicates that these landscape types can improve the thermal comfort. The correlation coefficients between MTHI and PLAND of water bodies at four time points are higher than those of cropland and forest. So, the water bodies have a stronger effect on improving the thermal comfort than cropland and forest in summer. A negative correlation exists between MTHI and PLAND of built-up land with a high correlation coefficient, which indicates that the more area the built-up land occupied, the worse the thermal comfort is.

In winter, thermal comfort levels of the same kind of landscape change greatly at different time points. It is possible to analyze the reason for the weakening of the solar radiation that reaches the surface in winter and the specific weather conditions of the imaging time.

Furthermore, the built-up land is mainly composed of cement and concrete. The heat radiation has rapid cooling after heat absorption. The water content of the natural underlying surface of cropland, water bodies, and forest is high, which has the characteristics of slow heat release after endothermic. MTHI is positively correlated with PLAND of cropland at time points 1 and 4 with a low correlation coefficient and a negative correlation at time points 2 and 3, which indicates that cropland has a slight effect of heat preservation when the temperature is relatively high in winter. The effect disappears when the temperature is lower. MTHI is positively correlated with PLAND of forest at time points 2 and 4. Combined with Fig. 3, the forest with sunlight exposure can play the role of heat preservation.

In spring, MTHI is substantially positively correlated with PLAND of the built-up land, indicating that the area with built-up area is the most comfortable in this season. MTHI is substantially negatively correlated with PLAND of water bodies, which indicates that places with water are more uncomfortable. At four time points of spring, there is a slight difference in the correlation between MTHI and PLAND of forest, which may have occurred due to the weather.

##### 4.3.2. Correlation MTHI and landscape structure on the 2.5 km × 2.5 km grid

To calculate the correlation between MTHI and AI and DIVISION of different landscape types, the quantity of observations at four time points are designated as follows: cropland (447, 443, 415 and 423), forest (305, 308, 298 and 332), water (377, 377, 363 and 359), and built-up land (448, 451, 446 and 457). As shown in Tables 6 and 7, the effects of landscape structure on thermal comfort are presented.

**Table 7**Correlation between MTHI<sub>mean</sub> and DIVISION.

Landscape types	Time point 1			Time point 2			Time point 3			Time point 4		
	Winter	Spring	Summer									
Cropland	-0.185**	0.078	0.020	0.598**	-0.108*	-0.93*	0.447**	-0.060	0.223**	-0.107*	0.063	0.153**
Forest	0.075	-0.086	0.182**	-0.074	0.149**	0.277**	0.149*	-0.001	0.241**	-0.243**	0.296**	0.260**
Water	0.691**	0.666**	0.547**	-0.396**	0.708**	0.583**	-0.704**	0.812**	0.469**	0.668**	0.680**	0.673**
Built-up	-0.061	-0.566**	-0.690**	-0.489**	-0.562**	-0.624**	-0.188**	-0.575**	-0.774**	-0.16	-0.683**	-0.600**

\*\*A significant correlation at the level of 0.01 (bilateral).

\*A significant correlation at the level of 0.05 (bilateral).

In summer, MTHI has a negative correlation with AI values of water bodies, which indicates that a large water body area has functioned better at adjusting the thermal comfort. MTHI has a markedly positive correlation with AI values of built-up land, indicating that the more concentrated the built-up land is, the higher the comfort level is. Relative to AI, the correlation between DIVISION and thermal comfort achieved different conclusions. As shown in Table 7, in summer, MTHI has a positive correlation with DIVISION values of forest and water bodies, illustrating that the more fragmented the forest and water bodies are, the worse the thermal comfort is. MTHI has a substantially negative correlation with DIVISION values of built-up land, indicating that the more discrete the built-up land is, the better the thermal comfort is. MTHI has a lower correlation with DIVISION values of cropland, which indicates that the discrete distribution of cropland can not affect the thermal comfort.

In winter, there is a lack of prominent characteristics of the correlation between MTHI and AI values. In spring, MTHI has a negative correlation with the AI values of water bodies. It illustrates that the more concentrated the water body is, the worse the thermal comfort is. In contrast to water bodies, MTHI has a positive correlation with AI values of built-up land, which illustrates that the more concentrated the built-up land is, the better the thermal comfort is.

#### 4.4. The extent of impacts of different landscape metrics on urban thermal comfort on the micro-scale

At the 2.5 km scale, the total variance contribution rate of three landscape metrics used in Section 4.3 to the mean value of MTHI is higher (74.1%–80.6%) (Table 8) that indicates that the composition and structure of landscape can create a better interpretation of the MTHI. The variance contribution rate of PLAND to MTHI is above 70%, and that of DIVISION and the AI is relatively low at between 10% and 38.1%, which illustrates that PLAND has the strongest explanatory ability of MTHI, which is the main landscape factor affecting urban thermal comfort. AI and DIVISION can also provide a certain interpretation of MTHI. Compared to PLAND, these factors are secondary landscape factors. Therefore, for urban thermal comfort, the composition of the landscape is the main affecting factor and is better than the structure of the landscape.

## 5. Discussion

### 5.1. The potential of the remote sensing-based temperature-humidity index

A thorough understanding of urban thermal comfort is particularly important because people need a comfortable thermal environment. The meteorological observation is usually used to evaluate the urban thermal comfort in the previous research, which has the advantage of continuous observation over a long period and can be used to calculate the temperature-humidity indexes on different time scales. By exploiting the meteorological data, the temporal evolution of thermal comfort may be obtained but has limitations in spatial analysis. Using remote sensing technology can give the illustration on reflecting the spatial characteristics of the thermal comfort. Two key steps are shown as follows:

**Table 8**

The variance contribution rate of different landscape metrics to MTHI.

Landscape metrics	Variance contributes rate (%)			
	Time point 1	Time point 2	Time point 3	Time point 4
PLAND	70.7	78.8	79.2	75.0
DIVISION	10.0	10.6	25.7	23.7
AI	30.7	27.1	38.1	24.6
Total	74.1	80.1	80.6	76.9

- 1) Innovating THI. The Modified Temperature-Humidity Index (MTHI) is established to reflect the spatial-temporal changes of urban thermal comfort by Land Surface Temperature (LST) and Normalized Moisture Index (NDMI) retrieved from Landsat TM, ETM+, TIRS/OLI data. From the spatial perspective, the spatial changes in urban thermal comfort in 2013 are explored (Fig. 10). The other advantage of using remote sensing data is the potential to reflect the temporal characteristics of the thermal comfort on different spatial scales. Fig. 11 shows the annual variations of the thermal comfort levels in the studied area where only the summer is included because it is the season with the most discomfort in Nanjing. This new temperature-humidity index based on remote sensing data can not only monitor the spatial distribution and temporal variations of urban thermal comfort levels at the macro scale but also can explain the reasons for the spatial-temporal variations of the thermal comfort at the micro scale.
- 2) Grading the thermal comfort. Obtaining urban thermal comfort levels based on MTHI is the second key step for remote sensing based thermal comfort research. Rational grading can directly affect the following work.

Based on these two steps, help of landscape metrics, the impact of landscape patterns on urban thermal comfort annually and seasonally is analyzed quantitatively. The characteristics of thermal environment are mainly determined by the types of patches, but the size and shape of the patches have different degrees of influence on them. The conclusions can provide reference for urban planning.

### 5.2. Further work for urban thermal comfort based on remote sensing data

Despite the great potential of the remote sensing-based index and grading, an issue is the availability of remote sensing data. Only several images are available in a season, and these cannot fully represent the thermal comfort of a season. In this study, the abnormal values can be found. For example, the comfort levels in the southern part of Jiangning District and in the southwest part of Pukou District presented abnormal. The potential reasons include the following: 1) the data are not sufficient, which can only reflect the situation at one time and not for the whole season; and 2) thermal comfort here is a relative value, which only reflects the thermal comfort level of one location relative to the remainder of locations in the study area. Fortunately, the increasing capability of satellites in a revisit can provide a more reliable investigation. In further work, the denser archive optical data (MODIS products) will be used to show the spatial and temporal difference in urban thermal comfort in typical cities on the Global scale or in different cities in China.

The other limitation of this study is that only the relative urban thermal comfort levels on the spatial scale can be achieved. Comparisons in time and among different cities are questionable. The next target is how to obtain the universal formula for calculating the thermal comfort such as the traditional comfort index.

For the study of thermal comfort, it is also important to study the scale-effect of landscape patterns on urban thermal comfort levels. Therefore, in the ensuing work, the high-resolution remote sensing image is used to select typical regions for studying the relationship between humidity-temperature indexes and the landscape pattern. Finally, the landscape configuration is obtained that is most beneficial to urban thermal comfort.

## 6. Conclusions

The modified temperature-humidity index indicated the spatial details of the urban thermal comfort, which can not only monitor spatial distribution and temporal variation of urban thermal comfort levels at the macroscale but can also explain the reasons for the spatial-temporal variations of thermal comfort on the micro scale. Combined

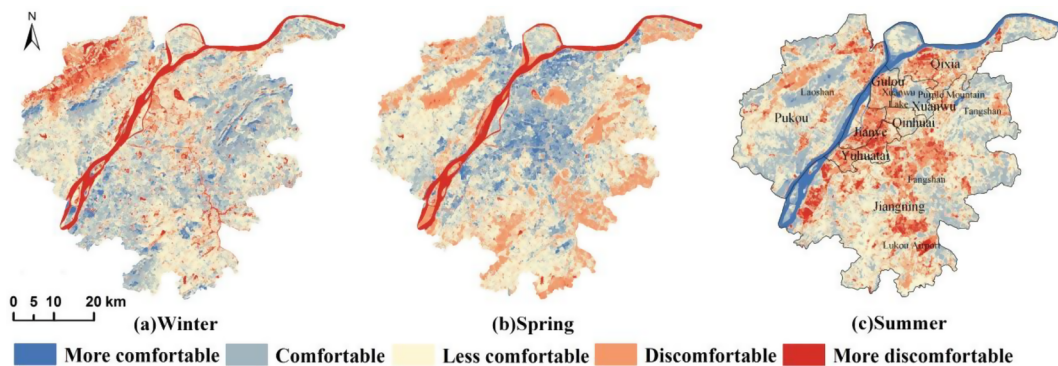


**Fig. 10.** Seasonal changes of thermal comfort levels in 2013 in study area.

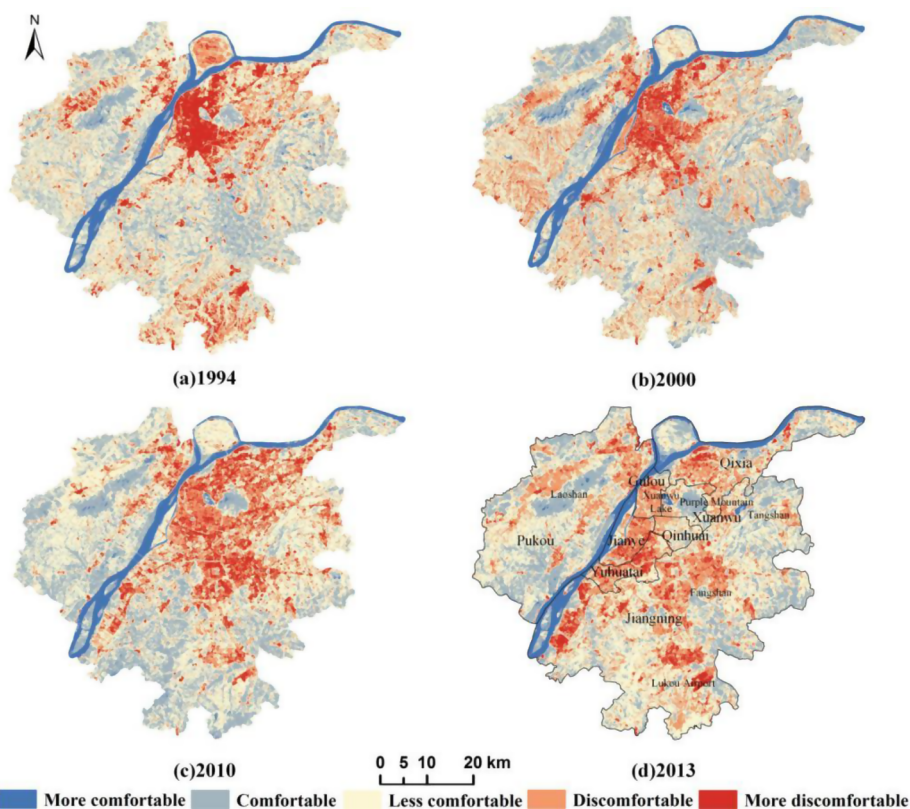


**Fig. 11.** Annual changes of thermal comfort levels in study area.

with landscape metrics, a preliminary quantitative analysis has been conducted on the relationship between the landscape composition and structure and thermal comfort.

### Acknowledgments

This research was supported by “the National Natural Science Foundation of China under Grant 41771446 and 41871326”, and “the Fundamental Research Funds for the Central Universities under Grant 2018B18414” and “the National Key Research and Development Program under Grant 2016YFA0601500 approved by Ministry of Science and Technology”. The authors would like to thank all the organizations for sharing data.

## References

- Fanger, P.O., 1970. Thermal Comfort: Analysis and Applications in Environmental

- Engineering. Danish Technical Press, Copenhagen, Denmark.
- Han, J., Zhang, G., Zhang, Q., et al., 2007. Field study on occupants' thermal comfort and residential thermal environment in a hot-humid climate of China. *Build. Environ.* 42 (12), 4043–4050.
- Hardisky, M.A., Klemas, V., Smart, R.M., 1983. The influence of soil salinity, growth form, and leaf moisture on the spectral radiance of *Spartina alterniflora* canopies. *Photogramm. Eng. Remote Sens.* 49 (1), 77–84.
- He, X.D., Miao, S.G., Shen, S.H., et al., 2015. Influence of sky view factor on outdoor thermal environment and physiological equivalent temperature. *Int. J. Biometeorol.* 59 (3), 285–297.
- Houghton, F.C., Yaglou, C.P., 1923. Determining equal comfort lines. *J. Am. Soc. Heat. Ventilat. Eng.* 29, 165–176.
- Horikoshi, T., Tsuchikawa, T., Kurazumi, Y., Matsubara, N., 1995. Mathematical expression of combined and separate effect of air temperature, humidity, air velocity and thermal radiation on thermal comfort. *Arch. Complex Environ. Stud.* 7 (3–4), 9–12.
- Höppe, P., 1999. The physiological equivalent temperature—A universal index for the biometeorological assessment of the thermal environment. *Int. J. Biometeorol.* 43, 71–75.
- Huynh, C., Eckert, R., 2012. Reducing heat and improving thermal comfort through urban design—a case study in Ho Chi Minh city. *Int. J. Environ. Sci. Dev.* 3, 480–485.
- Hu, Y., Li, P., Yang, J.G., et al., 2005. Applied meteorology. China Meteorological Press, Beijing, pp. 194.
- Kakon, A.N., Nobuo, M., Kojima, S., Yoko, T., 2010. Assessment of thermal comfort in respect to building height in a high-density city in the tropics. *Am. J. Eng. Appl. Sci.* 3 (3), 545–551.
- Li, X.T., Yu, Z., Zhao, B., Li, Y., 2005. Numerical analysis of outdoor thermal environment around buildings. *Build. Environ.* 40, 853–866.
- Lin, T.P., Matzarakis, A., Hwang, R.L., 2010. Shading effect on long-term outdoor thermal comfort. *Build. Environ.* 45, 213–221.
- Li, S.F., Qian, L.X., Wang, J., 2013. Improved Temperature-Humidity Index based on Landsat TM/ETM+ and its response to impervious surface. *Geogr. Geo-Inf. Sci.* 29 (2), 112–115 (in Chinese).
- Matzarakis, A., Mayer, H., Iziomon, M.G., 1999. Applications of a universal thermal index: physiological equivalent temperature. *Int. J. Biometeorol.* 43, 76–84.
- Makaremi, N., Salleh, E., Jaafer, M.Z., Ghaffarianhoseini, A.H., 2012. Thermal comfort conditions of shaded outdoor spaces in hot and humid climate of Malaysia. *Build. Environ.* 48, 7–14.
- Middel, A., Hab, K., Brazel, A.J., Martin, C.A., Guhathakurta, S., 2014. Impact of urban form and design on mid-afternoon microclimate in Phoenix Local Climate Zones. *Landscape Urban Plann.* 122, 16–28.
- Nagano, K., Horikoshi, T., 2011. Development of outdoor thermal index indicating universal and separate effects on human thermal comfort. *Int. J. Biometeorol.* 55 (2), 219–227.
- Nasir, R.A., Ahmad, S.S., Ahmed, A.Z., 2013. Perceived and measured adaptative thermal comfort at an outdoor shaded recreational area in Malaysia. *Adv. Mater. Res.* 610–613, 1083–1086.
- Nikolopoulou, M., Steemers, K., 2003. Thermal comfort and psychological adaption as a guide for designing urban spaces. *Energy Build.* 35, 95–101.
- Omonijo, A.G., 2017. Assessing seasonal variations in urban thermal comfort and potential health risks using Physiologically Equivalent Temperature: a case of Ibadan, Nigeria. *Urban Clim.* 21, 87–105.
- Parsons, K.C., 2013. Human Thermal Environments: The Effects of Hot, Moderate, and Cold Environments on Human Health, Comfort, and Performance, third ed. CRC Press, Taylor & Francis Group, New York.
- Peng, J., Xie, P., Liu, Y.X., et al., 2016. Urban thermal environment dynamics and associated landscape pattern factors: A case study in the Beijing metropolitan region. *Remote Sens. Environ.* 173, 145–155.
- Peng, J., Jia, J.L., Liu, Y.X., et al., 2018. Seasonal contrast of the dominant factors for spatial distribution of land surface temperature in urban areas. *Remote Sens. Environ.* 215, 255–267.
- Picot, X., 2004. Thermal comfort in Urban Spaces: Impact of Vegetation Growth: Case Study: Piazza Della Scienza, Milan, Italy. *Energy Build.* 36 (4), 329–334.
- Qin, Z.H., Karnieli, A., Berliner, P., 2001. A mono-window algorithm for retrieving land surface temperature from Landsat TM data and its application to the Israel-Egypt border region. *Int. J. Remote Sens.* 22 (18), 3719–3746.
- Qiao, Z., Wu, C., Zhao, D., Xu, X., Yang, J., Feng, L., Sun, Z., Liu, L., 2019. Determining the Boundary and Probability of Surface Urban Heat Island Footprint Based on a Logistic Model. *Remote Sens.* 11, 1368.
- Steeneveld, G., Koopmans, S., Heusinkveld, B., Theeuwes, N., 2014. Refreshing the role of open water surfaces on mitigating the maximum urban heat island effect. *Landscape Urban Plann.* 121, 92–96.
- Sun, S.B., Xu, X.Y., Lao, Z.M., et al., 2017. Evaluating the impact of urban green space and landscape design parameters on thermal comfort in hot summer by numerical simulation. *Build. Environ.* 123, 277–288.
- Toy, S., Kantor, N., 2017. Evaluation of human thermal comfort ranges in urban climate of winter cities on the example of Erzurum city. *Environ. Sci. Pollut. Res.* 24 (2), 1–10.
- Thorsson, S., Honjo, T., Lindberg, F., Eliasson, I., Lim, E.-M., 2007. Thermal comfort and outdoor activity in Japanese urban public places. *Environ. Behav.* 39, 660–684.
- Tselepidaki, I., Santamouris, M., Moustris, C., Poulopoulou, G., 1992. Analysis of the summer discomfort index in Athens, Greece, for cooling purposes. *Energy Build.* 18 (1), 51–56.
- Thom, E.C., Bosen, J.F., 1959. The discomfort index. *Weatherwise* 12, 57–61.
- Vancutsem, C., Ceccato, P., Dinku, T., Connor, S.J., 2010. Evaluation of MODIS land surface temperature data to estimate air temperature in different ecosystems over Africa. *Remote Sens. Environ.* 114 (2), 449–465.
- Wang, Y.F., Groot, R., Bakker, F., et al., 2017. Thermal comfort in urban green spaces: a survey on a Dutch university campus. *Int. J. Biometeorol.* 61, 87–101.
- Weng, Q.H., 2009. Thermal infrared remote sensing for urban climate and environmental studies: method, applications, and trends. *ISPRS J. Photogramm. Remote Sens.* 64 (4), 335–344.
- Wu, J.G., 2007. Landscape ecology-pattern, process, scale and hierarchy, 2nd ed. Higher Education Press, Beijing.
- Xu, H.Q., Hu, X.J., Guan, H.D., He, G.J., 2017. Development of a fine-scale discomfort index map and its application in measuring living environments using remotely-sensed thermal infrared imagery. *Energy Build.* 150, 598–607.
- Yaglou, C.P., Minard, D., 1957. Control of heat casualties at military training centers. *Am. Med. Assoc. Arch. Ind. Health* 16, 302–316.
- Yang, X.S., Zhao, L.H., Bruse, M., Meng, Q.L., 2013. Evaluation of a microclimate model for predicting the thermal behavior of different ground surfaces. *Build. Environ.* 60, 93–104.
- Yu, W., Liu, M.S., Xu, C., et al., 2007. The characteristic scales of the urban landscape in the Nanjing metropolitan region. *Acta Ecol. Sinica* 27 (4), 1480–1488 (in Chinese).
- Zauli, S.S., Tibaldi, S., Scotto, F., Lauriola, P., 2008. Bioclimatic characterization of an urban area: a case study in Bologna (Italy). *Int. J. Biometeorol.* 52 (8), 779–785.
- Zhang, Y., Yu, T., Gu, X.F., et al., 2006. Land surface temperature retrieval from CBERS-02 IRM SS thermal infrared data and its applications in quantitative analysis of urban heat island effect. *J. Remote Sens.* 10 (5), 789–797.
- Zhang, Y., Jiang, P., Chen, Y.Y., et al., 2012. Study on heat island effect in Wuhan city based on Landsat TM remote sensing. *Ecol. Environ. Sci.* 21 (5), 884–889 (in Chinese).
- Zhang, B., Wang, C.P., Shen, Y.L., Liu, Y.L., 2018. Fully connected conditional random fields for high-resolution remote sensing land use/land cover classification with convolutional neural networks. *Remote Sens.* 10 (12), 1889.
- Zou, Y., Greenberg, J.A., 2019. A spatialized classification approach for land cover mapping using hyperspatial imagery. *Remote Sens. Environ.* 232, 1–9.